Nanoscale

RSC Publishing

COMMUNICATION

Phase change nanocomposites with tunable melting temperature and thermal energy storage density†

Cite this: *Nanoscale*, 2013, **5**, 7234

Minglu Liu and Robert Y. Wang*

Received 31st May 2013
Accepted 28th June 2013

DOI: 10.1039/c3nr02842a

www.rsc.org/nanoscale

Size-dependent melting decouples melting temperature from chemical composition and provides a new design variable for phase change material applications. To demonstrate this potential, we create nanocomposites that exhibit stable and tunable melting temperatures through numerous melt–freeze cycles. These composites consist of a monodisperse ensemble of Bi nanoparticles (NPs) embedded in a polyimide (PI) resin matrix. The Bi NPs operate as the phase change component whereas the PI resin matrix prevents nanoparticle coalescence during melt–freeze cycles. We tune melting temperature and enthalpy of fusion in these composites by varying the NP diameter. Adjusting the NP volume fraction also controls the composite's thermal energy storage density. Hence it is possible to leverage size effects to tune phase change temperature and energy density in phase change materials.

The origins of size-dependent melting arise from the increasing surface to volume ratio as a material's characteristic length decreases.[1–6] This size effect has been studied for over a century, starting with the theoretical work by Pawlow[7] and the experimental observation done by Takagi.[8] Buffet and Borel later used scanning electron diffraction to demonstrate that the melting temperature of gold can be varied by as much as ~500 °C.[9] Their data and thermodynamic model indicate that the decrease in melting temperature of nanoparticles depends inversely on nanoparticle diameter. This size-dependent melting phenomenon has since become known as melting point depression. Several other models and simulation results have since been conducted[5,6,10–12] and many other experimental observations have been reported: particles have been melted on substrate surfaces,[13–15] inside crystalline materials[16–18] and inside amorphous materials.[19–23] Lai *et al.*[24] used nanocalorimetry measurements to show that a decrease in enthalpy of fusion also accompanies melting point depression.

The majority of research on melting point depression largely focuses on nanoparticles formed *via* dewetting of vapor-deposited metals on substrates. While this production approach is sufficient for fundamental studies, it has limited value for practical applications. Technological applications that leverage melting point depression will simultaneously require scalable nanoparticle synthesis, particle size distribution control, and particle stability. Scalable nanoparticle syntheses such as ball milling,[25] melt spinning[19,23,26,27] and ion implantation[18,20] have been used, but yield broad particle size distributions and consequently poor

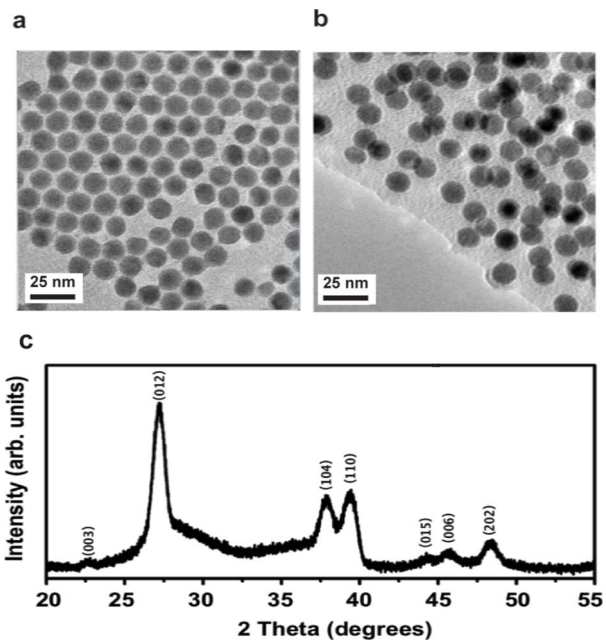

Fig. 1 (a) TEM image of Bi NPs with 14.5 nm diameter. (b) TEM image of a nanocomposite consisting of a PI resin matrix with embedded 14.5 nm diameter Bi NPs. The backgrounds in the top-right and bottom-left of the image correspond to PI resin and vacuum, respectively. (c) XRD pattern of 14.7 nm Bi NPs.

Mechanical Engineering, Arizona State University, Tempe, USA. E-mail: rywang@asu.edu

† Electronic supplementary information (ESI) available: Experimental details and additional DSC data on nanocomposites and pure PI resin. See DOI: 10.1039/c3nr02842a

control over melting characteristics. It is also important to isolate the particles from one another to prevent coalescence and preserve size-effects over numerous melt–freeze cycles.

To demonstrate a new approach to these challenges, we use solution-phase chemistry to create nanocomposites consisting of monodisperse Bi NPs dispersed in a PI resin matrix. Solution-phase synthesis of colloidal NPs presents a scalable production approach that exhibits excellent control over NP size, shape, and composition.[28–30] The PI resin matrix was chosen to prevent NP coalescence during melt–freeze cycles because it is a thermoplastic polymer with a glass transition temperature above the Bi melting temperature. The nanocomposites were made using a simple three-step approach: (a) synthesis of colloidal Bi NPs, (b) co-dissolution of Bi NPs and PI resin into a shared solvent, and (c) drop-casting onto an appropriate substrate. Adjusting the reaction conditions of the NP synthesis enabled control over NP size. Varying the ratio of NPs to PI resin in the shared solvent allows control over the composite's NP volume fraction. The monodisperse NPs produced by this approach can be seen in Fig. 1a and c, which show a transmission electron microscope (TEM) image and X-ray diffraction (XRD) pattern of typical Bi NPs. Fig. 1b is a TEM image of the nanocomposite formed by combining the Bi NPs with PI resin. This modular sample preparation approach enables melting-point depression studies in 3-dimensional composites with carefully controlled nanoparticle size, shape, and composition. This approach also has the practical advantage of producing sample quantities large enough to be studied with a standard differential scanning calorimeter (DSC). This circumvents the necessity of highly sophisticated *in situ* electron microscopy melting and microfabricated nanocalorimeter methods, which have been the standard melting point depression research tools.[4,6,13,14,20,24,31]

The Bi NPs were prepared by reducing $Bi[N(SiMe_3)_2]_3$ with hexadecylamine in the presence of $Li[N(SiMe_3)_2]$ and $Li(Et_3BH)$ as described by Yarema *et al.*[32] Varying the reaction temperature and amount of $Li(Et_3BH)$ allowed control over NP size. The NPs were cleaned by precipitating in ethanol several times and then dissolved in tetrahydrofuran (THF). The NPs produced in this synthesis consist of a Bi core with organic ligands that bind to the surface and act as a surfactant. To measure the true Bi-content of the NP solution (as opposed to the combined content of the Bi and ligands), we used a DSC method. In brief, a sample of NPs were drop-cast into a DSC pan and then subjected to multiple melt–freeze cycles. During this process, the NPs coalesce into a bulk material because the organic ligands are insufficient at isolating the NPs from one another. Consequently a melting valley at the bulk Bi melting temperature (271 °C) is observed. The Bi mass was determined by comparing this valley to the enthalpy of fusion for bulk Bi (51.9 J g^{-1}). To make the nanocomposite, PI resin was dissolved in THF in a separate container. Appropriate amounts of the NP solution and PI resin solution were then combined and drop-cast into a DSC pan. DSC measurements were carried out by cyclic heating and cooling between 0 °C and 300 °C at a rate 10 °C min^{-1}. More experimental details can be found in the ESI.†

Fig. 2a shows a typical heating and cooling cycle of a nanocomposite containing Bi NPs with 9.6 nm diameters. One endothermic valley and two exothermic peaks are observed during heating and cooling, respectively. We attribute the endothermic valley to NP melting. As expected this occurs well below the bulk melting temperature of Bi, which is 271 °C. We attribute the two exothermic peaks during cooling to two separate freezing events because the total energy released at these temperatures is equivalent to the energy absorbed during melting. These freezing events occur below the melting temperature, which is a common phenomenon known as supercooling. These melting and freezing assignments in the DSC data are corroborated by control measurements on pure PI resin, which showed no discernable features throughout the 0–300 °C temperature range (ESI Fig. S1†).

One major benefit of using nanoparticles for phase change applications is that their melting temperature can be tuned independently of their chemical composition. We demonstrate this by examining composites with Bi volume fractions of ~9.0–9.5%, but varying NP diameters: 7.8 ± 0.5, 9.6 ± 0.5, 13.2 ± 0.7,

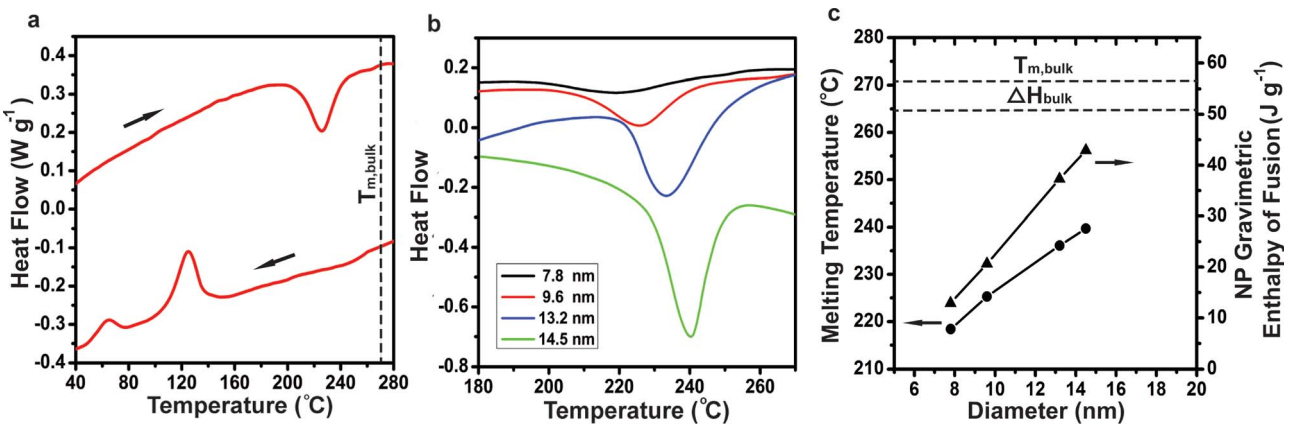

Fig. 2 (a) A heating and cooling DSC cycle for a composite with Bi NPs of 9.6 nm diameter. (b) The endothermic melting valley during DSC measurements for composites with Bi NPs of four different diameters. For clarity, the data in part (b) has been offset along the vertical axis. Each tick mark represents 0.1 W g^{-1}. (c) Size dependent melting temperature (circles) and enthalpy of fusion (triangles) for nanocomposites with Bi NPs of four different diameters.

and 14.5 ± 0.6 nm. As the NP diameter was varied from 7.8 to 14.5 nm, the melting temperature varied from 218 to 240 °C (Fig. 2b and c). Our observations indicate that the NP diameter and melting point depression magnitude are inversely proportional, which is in agreement with prior work.[9,31] Studies by Lai *et al.*[24] have previously shown that a decrease in enthalpy of fusion accompanies melting point depression. Due to the small NP signal, their studies required specialized microfabricated nanocalorimeters.[24] Since our NP synthesis approach produces large quantities of monodisperse particles, we are able to make this size-dependent enthalpy of fusion observation using a standard DSC. As the NP diameter varied from 7.8 to 14.5 nm, the NP enthalpy of fusion changed from 12.9 to 42.1 J g^{-1}. For clarity we now note that this communication refers to two different enthalpies of fusion throughout its text. The first is the NP gravimetric enthalpy of fusion, which corresponds only to the mass of the composite's Bi component. The second is the composite's volumetric enthalpy of fusion, which corresponds to the combined volume of the Bi and PI resin.

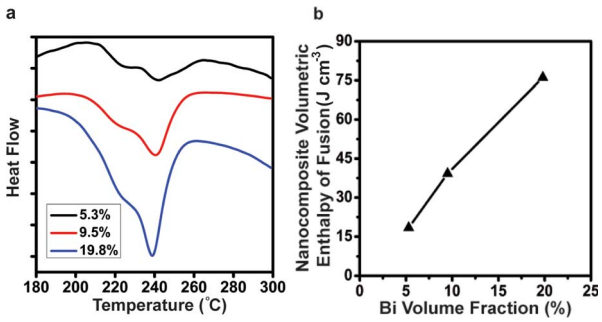

Fig. 3 (a) The endothermic melting valley during DSC measurements for composites with 14.7 nm diameter NPs and varying Bi volume fraction. For clarity, the data in part (a) has been offset along the vertical axis. Each tick mark represents 0.1 W cm^{-3}. (b) The composite's volumetric enthalpy of fusion for varying Bi volume fractions.

For practical applications, it may be desirable to tune the composite's enthalpy of fusion independently of melting temperature. To demonstrate this capability, we created composites with Bi NPs of 14.7 ± 0.5 nm diameter and varied the Bi volume fraction from 5.3% to 19.8%. As the volume fraction increased, the composite volumetric enthalpy of fusion increased proportionately and no discernable effect on melting temperature is observed (Fig. 3). This volume fraction design variable enables the composite's melting temperature and enthalpy of fusion to be independently controlled by a simple two-step process. First, the NP size is chosen to yield the desired melting temperature. Second, the Bi volume fraction is chosen to yield the desired composite volumetric enthalpy of fusion. The Bi volume fraction can be successfully increased to ~30%, however at ~41% bulk melting characteristics developed during thermal cycling (ESI Fig. S2†). Hence this represents an upper limit on the Bi volume fraction for which the PI resin matrix no longer prevents NP coalescence.

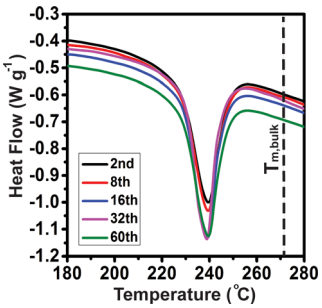

Fig. 4 Several representative heating cycles during cyclic DSC measurements on a composite with 14.5 nm Bi NPs.

Numerous melt–freeze cycles conducted on the nanocomposites demonstrate that the PI resin matrix is effective at preventing nanoparticle coalescence, which indicates that this approach could be used for technological applications. Despite subjecting the nanocomposite to 60 melt–freeze cycles, no notable changes in melting temperature or enthalpy of fusion were observed (Fig. 4). This is in stark contrast to previous literature results in which bulk-like behavior can even be observed during the first thermal cycle.[33,34] We note that while the PI resin matrix was sufficient at preventing nanoparticle coalescence, it was not sufficient at preventing oxidation. The Bi NPs in the nanocomposite were slowly oxidized over a period of weeks under ambient conditions. This can be addressed by choosing alternative matrix materials. Unlike previous experiments that use composites with polydisperse nanoparticles and ill-defined melting temperatures, these experiments demonstrate the feasibility of creating composites with monodisperse nanoparticles and well-defined melting temperature.

One application where these nanocomposites could excel is as a phase change material for thermal energy storage and thermal management. Latent heat is commonly used to store thermal energy because enthalpies of fusion are typically on the order of 10^2 °C of sensible heat.[35,36] In the low temperature regime (<80 °C), paraffin is commonly used for latent heat storage. One of paraffin's attractive qualities is that its melting temperature can be tuned, which is typically difficult with conventional materials. As the length of the paraffin's carbon chain is decreased, its melting temperature decreases.[37] In this respect, the Bi NP diameter plays a similar role to paraffin length. Furthermore, melting point depression is a general phenomenon and we see no reason why this nanocomposite approach cannot be generalized to other NP compositions. Hence NPs can provide thermal storage functionality and flexibility at temperatures above 80 °C where paraffin is not a viable option. In addition to accessing a temperature regime unattainable to paraffin, these composites also benefit from high volumetric enthalpies of fusion. For example, the nanocomposite with a 19.8% volume fraction of 14.7 nm NPs has a volumetric enthalpy of fusion that is ~100% greater than a typical paraffin such as RT60 (76 J cm^{-3} *vs.* 37 J cm^{-3}).[38]

This work demonstrates that polymer matrices can stabilize cyclic melting of NP ensembles and enable melting point depression studies in composites with carefully controlled nanoparticle size. This stabilized melting point depression also

creates possibilities for applications in phase change materials. For example, engineered thermal storage materials should be possible because melting temperature and enthalpy of fusion can be independently tuned by varying the composite's NP size and volume fraction.

Acknowledgements

This work was supported by the National Science Foundation through Grant no. CBET-1236656. We gratefully acknowledge the use of facilities within the LeRoy Eyring Center for Solid State Science at Arizona State University. We also thank Lenore Dai from Arizona State University for helpful discussions.

Notes and references

1 R. W. Cahn, *Nature*, 1986, **323**, 668.
2 J. W. M. Frenken and J. F. Vanderveen, *Phys. Rev. Lett.*, 1985, **54**, 134.
3 J. W. M. Frenken, P. M. J. Maree and J. F. Vanderveen, *Phys. Rev. B: Condens. Matter Mater. Phys.*, 1986, **34**, 7506.
4 R. Kofman, P. Cheyssac, A. Aouaj, Y. Lereah, G. Deutscher, T. Bendavid, J. M. Penisson and A. Bourret, *Surf. Sci.*, 1994, **303**, 231.
5 P. R. Couchman and W. A. Jesser, *Nature*, 1977, **269**, 481.
6 C. R. M. Wronski, *Br. J. Appl. Phys.*, 1967, **18**, 1731.
7 P. Pawlow, *Z. Phys. Chem.*, 1909, **65**, 545.
8 M. Takagi, *J. Phys. Soc. Jpn.*, 1954, **9**, 359.
9 P. Buffat and J. P. Borel, *Phys. Rev. A: At., Mol., Opt. Phys.*, 1976, **13**, 2287.
10 L. H. Liang, J. C. Li and Q. Jiang, *Physica B*, 2003, **334**, 49.
11 F. G. Shi, *J. Mater. Res.*, 1994, **9**, 1307.
12 H. M. Lu, P. Y. Li, Z. H. Cao and X. K. Meng, *J. Phys. Chem. C*, 2009, **113**, 7598.
13 A. N. Goldstein, C. M. Echer and A. P. Alivisatos, *Science*, 1992, **256**, 1425.
14 E. A. Olson, M. Y. Efremov, M. Zhang, Z. Zhang and L. H. Allen, *J. Appl. Phys.*, 2005, **97**, 034304.
15 J. Hu, Y. Hong, C. Muratore, M. Su and A. A. Voevodin, *Nanoscale*, 2011, **3**, 3700.
16 C. J. Rossouw and S. E. Donnelly, *Phys. Rev. Lett.*, 1985, **55**, 2960.
17 J. Zhong, L. H. Zhang, Z. H. Jin, M. L. Sui and K. Lu, *Acta Mater.*, 2001, **49**, 2897.
18 N. B. Thoft, J. Bohr, B. Buras, E. Johnson, A. Johansen, H. H. Andersen and L. Sarholtkristensen, *J. Phys. D: Appl. Phys.*, 1995, **28**, 539.
19 R. Goswami and K. Chattopadhyay, *Appl. Phys. Lett.*, 1996, **69**, 910.
20 Q. Xu, I. D. Sharp, C. W. Yuan, D. O. Yi, C. Y. Liao, A. M. Glaeser, A. M. Minor, J. W. Beeman, M. C. Ridgway, P. Kluth, J. W. Ager, D. C. Chrzan and E. E. Haller, *Phys. Rev. Lett.*, 2006, **97**, 155701.
21 Q. S. Mei, S. C. Wang, H. T. Cong, Z. H. Jin and K. Lu, *Phys. Rev. B: Condens. Matter Mater. Phys.*, 2004, **70**, 125421.
22 F. Banhart, E. Hernandez and M. Terrones, *Phys. Rev. Lett.*, 2003, **90**, 185502.
23 J. Mu, Z. W. Zhu, H. F. Zhang, H. M. Fu, A. M. Wang, H. Li and Z. Q. Hu, *J. Appl. Phys.*, 2012, **111**, 043515.
24 S. L. Lai, J. Y. Guo, V. Petrova, G. Ramanath and L. H. Allen, *Phys. Rev. Lett.*, 1996, **77**, 99.
25 M. A. Meitl, T. M. Dellinger and P. V. Braun, *Adv. Funct. Mater.*, 2003, **13**, 795.
26 R. Goswami and K. Chattopadhyay, *Acta Mater.*, 2004, **52**, 5503.
27 E. Haro-Poniatowski, M. Jimenez de Castro, J. M. Fernandez Navarro, J. F. Morhange and C. Ricolleau, *Nanotechnology*, 2007, **18**, 315703.
28 J. Park, J. Joo, S. G. Kwon, Y. Jang and T. Hyeon, *Angew. Chem., Int. Ed.*, 2007, **46**, 4630.
29 A. R. Tao, S. Habas and P. D. Yang, *Small*, 2008, **4**, 310.
30 Y. N. Xia, Y. J. Xiong, B. Lim and S. E. Skrabalak, *Angew. Chem., Int. Ed.*, 2009, **48**, 60.
31 G. L. Allen, R. A. Bayles, W. W. Gile and W. A. Jesser, *Thin Solid Films*, 1986, **144**, 297.
32 M. Yarema, M. V. Kovalenko, G. Hesser, D. V. Talapin and W. Heiss, *J. Am. Chem. Soc.*, 2010, **132**, 15158.
33 K. Dick, T. Dhanasekaran, Z. Y. Zhang and D. Meisel, *J. Am. Chem. Soc.*, 2002, **124**, 2312.
34 C. Tang, Y.-M. Sung and J. Lee, *Appl. Phys. Lett.*, 2012, **100**, 201903.
35 B. Zalba, J. M. Marin, L. F. Cabeza and H. Mehling, *Appl. Therm. Eng.*, 2003, **23**, 251.
36 A. Sharma, V. V. Tyagi, C. R. Chen and D. Buddhi, *Renewable Sustainable Energy Rev.*, 2009, **13**, 318.
37 P. J. Flory and A. Vrij, *J. Am. Chem. Soc.*, 1963, **85**, 3548.
38 R. Velraj, R. V. Seeniraj, B. Hafner, C. Faber and K. Schwarzer, *Solar Energy*, 1999, **65**, 171.

